Identifying Oil Spill Types Based on Remotely Sensed Reflectance Spectra and Multiple Machine Learning Algorithms

Ying Li, Qinglai Yu, Ming Xie, Zhenduo Zhang, Zhanjun Ma, and Kai Cao

***Abstract*—An accurate identification of oil spill types is the basis of determining the source of leakage, evaluating the potential damage, and deciding a plan of responses for an oil spill event. Despite sufficient studies that interpreted and analyzed hyperspectral data of oil spills, these studies that identify or classify oil spill types is rather limited. Aiming at identifying different types of oil spills, this article analyses the reflectance spectra obtained from high-resolution hyperspectral sensors using multiple machine learning methods. Four types of machine learning models are applied in this article: random forest; support vector machine (SVM); and deep neural network (DNN); and DNN with differential pooling (DP-DNN). The training and testing data are collected by field experiments under different environmental condition in order to verify the robustness of the machine learning models. The characteristics of reflectance is briefly described, and the results conform with results from previous studies. The performances of the machine learning models are evaluated and compared in terms of both accuracy of prediction and computational complexity. The results indicate that the two DNN models are able to achieve the most accurate prediction among the four machine learning models at the cost of more computation. The SVM model, or the proposed DP-DNN model may be a favorable choice when training time is limited.**

***Index Terms*—Hyperspectral remote sensing, machine learning, oil spill, oil type identification.**

I. Introduction

OIL leakage from various sources results in different types of oil spills [1]. For examples, natural leakage or leakage from ports or platforms is dominated by crude oil, while that caused by the emission or collision of ships is more likely to be fuel or engine oil. Therefore, an accurate identification of oil spill types can help determine the source of leakage, potential damage, and decide a plan of response [2].

Despite sufficient studies in the area of petroleum hydrocarbons (PHCs) spill monitoring [3], the studies that identify or classify the oil spill types is rather limited. Chemical methods, such as chromatographic or mass spectroscopic analysis on oil samples, can provide accurate inferences on oil spill types [4], [5]. Some studies also suggested that oil types could be recognized through laser induced fluorometric spectra [6], [7]. However, these methods usually require in situ sampling, and could be costly or time-consuming.

Owing to its advantage of high efficiency, remote sensing technology has been applied in the area of PHCs spill monitoring to obtain and interpret information about PHC pollutants. Specifically, the potential of hyperspectral sensor, which records a continuous spectrum of high dimensionality and resolution, is highly considered [8]–[10]. The spectral response of oil slick has been measured and analyzed in sufficient previous studies. Clark *et al*. [11] developed an imaging spectroscopy system called "Tetracorder" for material identification and mapping. Their team measured and analyzed reflectance spectra of alkanes [12], and developed a method for mapping oil spill thickness using imaging spectroscopy [13]. Lu *et al*. studied the reflectance spectra of offshore oil slick and observed an absorption peak at around 750 nm and a reflection peak at around 820 nm [14]. This result also conformed with the measurements by other researchers [1], [15], [16].

Analyzing hyperspectral imagery (HSI) using machine learning algorithms has become a trend in recent studies. As a powerful tool of recognizing spatial patterns in images, convolutional neural network (CNN) has been applied to the field of object classification in hyperspectral remote sensing [17], [18]. In term of oil spill detection, researchers have developed various models using CNN to extract the oil spill zone in HSI [19], [20], and estimate oil spill thickness [21]–[23]. Nevertheless, the study that addresses the identification of oil types using passive hyperspectral remote sensing method is still insufficient. Oil-type identification is a fine-grained classification problem that tries to distinguish between different types of oil, which show very similar pattern in reflectance spectra and are usually classified as one category in the traditional HSI classification method. Like other fine-grained classification problem [24], oil type identification also encounters the difficulty of classifying foreign bodies with identical spectra. A recent study by Yang *et al*. [1] analyzed the characteristics of reflectance spectra for different types of oil, and tried to classify their types using support vector machine (SVM).

This article aims at the identification of oil types by recognizing the intrinsic pattern in the reflectance spectra using

Manuscript received January 27, 2021; revised April 6, 2021 and May 24, 2021; accepted August 31, 2021. Date of publication September 3, 2021; date of current version September 22, 2021. This work was supported in part by China National Key R&D Program under Grant 2020YFE0201500, Liaoning Revitalization Talents Program under Grant XLYC2001002, and China Postdoctoral Science Foundation under Grant 2020M670730. (*Corresponding author: Ming Xie*.)

The authors are with the Navigation College, Dalian Maritime University, Dalian 116026, China (e-mail: yldmu@dlmu.edu.cn; 1120191065@dlmu.edu.cn; mingxie@dlmu.edu.cn; zhangzhenduo@dlmu.edu.cn; mazhanjun@dlmu.edu.cn; caokai@dlmu.edu.cn).

Digital Object Identifier 10.1109/JSTARS.2021.3109951

This work is licensed under a Creative Commons Attribution 4.0 License. For more information, see https://creativecommons.org/licenses/by/4.0/

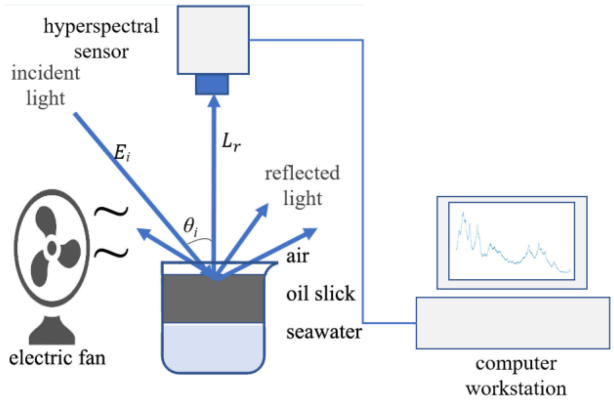

Fig. 1. Experiment set-up for hyperspectral measurements.

high-resolution hyperspectral sensor and advanced machine learning algorithm. Four types of machine learning methods are adopted to complete this objective. As a test to identify oil spill types through hyperspectral remote sensing, this article also evaluates the performances of some commonly-used machine learning models, and provides suggestions on the choices of methods for the analysis on the reflectance spectra of oil spill.

II. Methodology

A. Bidirectional Reflectance Distribution Function (BRDF) Model of Oil Slicks

The measurement and processing of oil slick reflectances is built on the theoretical basis of the BRDF, which is defined by Nicodemus [25] as the ratio of reflected light radiance per spherical angle over the incident light irradiance

$$\mathrm{BRDF}(\theta i, \varphi i, \theta r, \varphi r, \lambda) = \frac{dLr(\theta r, \varphi r, \lambda)}{dEi(\theta i, \varphi i, \lambda)} \tag{1}$$

where L_r is the measured radiance of target and E is the irradiance; θ is zenith angle and φ is azimuth angle; index i means the incident and r means reflected; and λ is the wavelength of incident light. From the microscopic point of view, BRDF is the ratio between the number of photons reflected in a small solid angle and that of the total incident photons. This concept is corresponding to the remote sensing reflectance, which is calculated as the ratio between water-leaving radiance and incident irradiance. Otremba and his team conducted a series of simulations and measurements on the BRDF characteristics of oil slick. They found that the radiance reflectances distribute symmetrically along the 0° azimuth plane, and are strongly affected by incident zenith angle [26]–[29].

In order to simulate the measurement from airborne or satellite-based remote sensing techniques, the reflectance of oil slick is measured with a hyperspectral sensor facing vertically down to the oil slick in this article (see Fig. 1). According the BRDF model discussed above, the obtained spectrum is the BRDF at 0 reflected zenith angle, while the illumination angle depends on the sunlight incident zenith angle at the time of the experiment.

A Lambertian body standard white plate is applied along with the hyperspectral sensor to measure and calculate spectral radiance and incident irradiance. The sensor is calibrated with standard plate before each measurement of spectral radiance of oil samples. The incident irradiance is calculated using the following equation:

$$E_i(\theta i, \varphi i, \lambda) = \frac{L_s(\theta r, \varphi r, \lambda)\pi}{\rho(\theta r, \varphi r, \lambda)} \tag{2}$$

where L_s is the measured radiance of standard plate, and ρ is the reflectivity of standard plate. The standard plate which is co 25% in this article.

B. Material Preparation and Experimental Scheme

The training and testing data for the machine learning models are collected through field experiments. Four types of oil that are likely to be witnessed in the oil spill events are selected as the object of identification and classification in this article.

1) Crude oil of black appearance and moderate viscosity. The physical property and chemical composition could vary for the crude oil produced in different places. The crude oil used in this article is produced in Saudi Arabia and collected from the Singaporean oil tanker LUSHAN.

2) #0 diesel, which is a commonly-used light ship fuel while sailing in river and nearshore area. Diesel has yellow appearance and is lighter in density compared with crude oil.

3) Lubricant (sometimes also referred as marine engine oil), which is usually applied to ship engine in order to resist the corrosion in engine part and extend the engine life. Lubricant also has yellow appearance and is lighter in density compared with crude oil. The lubricant used in this article is collected from the YUKUN ship.

4) Heavy diesel, which is a commonly-used heavy ship fuel while ocean-going. Heavy diesel has black appearance and high viscosity. Generally, crude oil and heavy diesel are two types of heavy oil, while diesel and lubricant are two types of light oil. Fig. 2 shows the appearances of these four types of oil samples.

In the experiments, oil samples are placed separately on freshly collected sea water in the beakers. The bottom and side of the beakers are painted as black in order to simulate the absorption of sea water. A hyperspectral sensor is mounted on a frame and faces vertically down to the oil sample. Previous studies indicated that the incident zenith angle, oil thickness, and wind condition would all affect the reflectance [27]–[30]. Thus, in order to test the robustness of machine learning models, the hyperspectral data is collected at different time (under different incident zenith angle) for nine sets of oil thickness (10.23 μm, 30.69 μm, 306.9 μm, 511.5 μm, 716.1 μm, 920.7 μm, 1.535 mm, 1.739 mm, and 1.944 mm) under both calm condition and artificial wind. The oil sample is dripped onto water surface using a dropper with scale, so the thickness of the oil sample is calculated based on the ratio of the oil volume and the surface area of the beaker. It is usually difficult to drip all the oil sample in the dropper due to its viscosity. Therefore, the oil volume is measured through the reduced volume in the dropper using the scale on the dropper. Considering the oil sample stuck on the

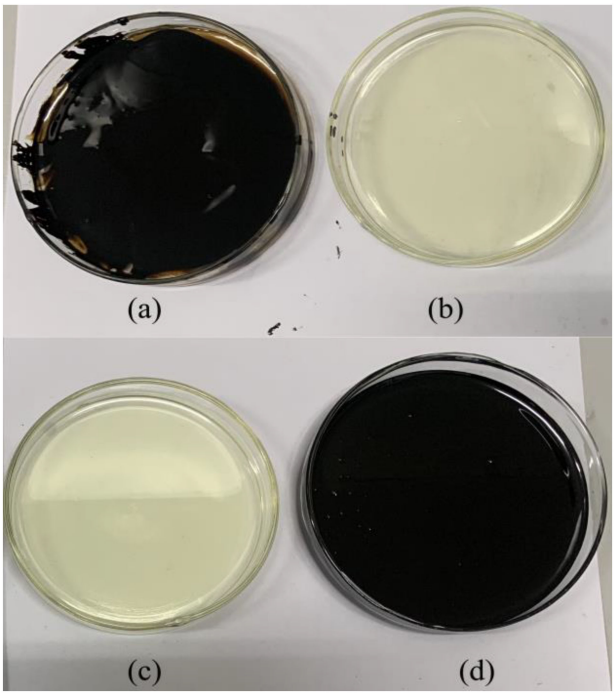

Fig. 2. Photograph of the oil samples. (a) Crude oil. (b) Diesel. (c) Lubricant. (d) Heavy diesel.

dropper wall, beakers with relatively large diameter (diameter: 129 mm; height: 468 mm; volume: 4000 ml) were used in the experiments in order to reduce the error in oil thickness calculation.

The beakers are painted as black in order to simulate the absorption of sea water, and then filled with 3600 ml freshly collected sea water (about 420 mm in depth, water temperature ranges from 21°C to 24°C). Oil samples are dripped onto the water surface and the irradiance measurements are not conducted until a stable oil film is formed. It usually takes about 1–3 min for the light oil to form a stable oil film, while heavy oil need to be warmed with hot water (about 70 °C) before using. The artificial wind is generated with an electric fan.

The hyperspectral sensor applied in this article is assembled based on Teledyne Lumenera Lt365R pushbroom camera, which takes a slit of 1456 pixels in each frame. The spectrum range of the camera is 392.00–1162.67 nm, with 1936 bands. The silicon response range of the camera lens is 200–1200 nm, which fully covers the spectral range used for classification in this article. In the experiment, the oil samples are placed in the center of the camera's vision field. Therefore, only the spectra in the center pixels are extracted for spectral analysis. The camera takes about 20 s of shoots at 10 ms exposure time (about 2000 slits) in each measurement and generates an HSI cube based on the measured slits. It should be noted that camera is placed statically on the oil sample. Therefore, the three dimensions of the generated HSI cubes are within spatial domain (1456 pixels in the direction of slit), temporal domain (about 2000 slits during each measurement), and spectral domain (1936 bands).

TABLE I
DATE AND TIME OF EXPERIMENTS, AS WELL AS CORRESPONDING SUN ELEVATION AND AZIMUTH ANGLES

Experiment Number	Date and time (UTC+8)	Sun elevation angle	Sun azimuth angle
1	4 Sept. 2019, 10:00	48.49°	131.5°
2	4 Sept 2019, 12:00	58.43°	180.0°
3	4 Sept 2019, 15:00	38.71°	244.1°
4	4 Sept 2019, 16:30	22.00°	261.3°

The experiments are conducted in outfield environment under sunlight during cloudless weather. The location of the experiment is at 38°52'18.4" N and 121°31'36.5" E. The date and time of the experiments and corresponding sun elevation/azimuth angles are given in Table I. Although the incident zenith angle, oil thickness, and wind condition are collected in the experiments for spectral analysis, they are not fed to the machine learning models in order to test whether the models are able to identify different types of oil without pre-knowledge about these conditions.

C. Machine Learning Algorithms and Implementation Details

Four types of machine learning algorithms are applied to the spectra data for oil types identification: random forest (RF); SVM; deep neural network (DNN); and (4) DNN with differential pooling (DP-DNN). The training and testing data for the machine learning models are obtained from the experiments described above. Specifically, a total of 190 frames of spectra are randomly chosen from the data collected for each type of oil (four in total) with each set of thickness (ninr in total) under each kind of wind condition (two in total). Thus, there are 13 680 frames of spectra in the dataset. 80% of the data are used for training, and 20% of the data are used for testing. The whole spectrum that consists of 1936 bands is considered as the input data, which are classified into four categories represents for the four types of oil. The machine learning models are constructed using statistical and machine learning Toolbox in MATLAB R2019a, and trained using 2.5 GHz Intel i5-7300 HQ CPU with 8.0 GB of RAM running on a 64-bit Windows 10 operating system. The codes of all the models used in this article is available at https://github.com/349898680/oil-type-identification-models. Model structure and detail implementations for the four machine learning algorithms are discussed in following sections.

1) Random Forest: As a classical method of machine learning, RF is a type of supervised-learning that consists of a number of tree-like classifiers and a majority vote [31]. In bagged RF, each classifier makes prediction based on its own decision tree. The votes from all classifiers are collected and the prediction with highest number of votes are considered as the final output [32]. RF is able to handle high data dimensionality and has been applied to the classification based on hyperspectral remote sensing data [33]. In this article, the RF model consists of 200 tree-like classifiers. The working flow of RF applied in this article is shown as Fig. 3(a).

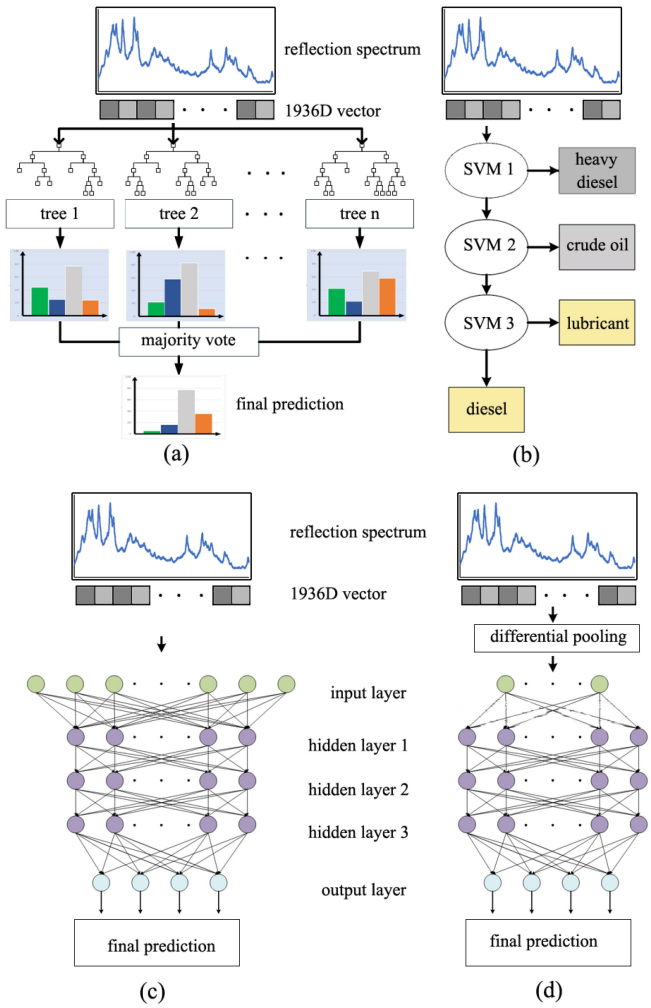

Fig. 3. Workflow of the four machine learning models. (a) Random forest. (b) Support vector machine. (c) Deep neural network. (d) DNN with differential pooling.

2) Support Vector Machine: Proposed by Cortes and Vapnik [34], SVM has proved to be a powerful classification tool and received fast development in the last two decades. The mechanism of SVM is to project the data points into a higher-dimension space through kernel function, and then separate the data points into two parts using a hyper-plane [35]. In this article, the radial basis function is adopted as the kernel function.

Although SVM is able to robustly handle the non-linear classification with relatively small number of calculations, it is intrinsically a binary classification [34]. In order to solve the multi-class classification methods, multiple classifiers need to be trained as One-versus-All (OVA, classifiers distinguish each class from the rest of the classes) or All-versus-All (AVA, classifiers distinguish two classes for each of the combinations). In this article, OVA is adopted in this article since it is able to provide reasonable classification results with less calculations [36]. Specifically, three classifiers are trained to complete the classification: the first classifier distinguishes heavy diesel from the rest types of oils; the second classifier distinguishes crude oil from the rest types of oils; the third classifier distinguishes between light diesel and lubricant. The workflow of SVM model applied in this article is shown as Fig. 3(b). It should be noted that the structure of the model is built according the number of classes. It may not be favorable for the classification tasks involving a greater number of classes.

3) Deep Neural Network: The appearance of DNN significantly propelled the development of artificial intelligence technology in the last decades. As shown in Fig. 3(c), the DNN model applied in this article is built based on a series of fully-connected layers, which include an input layer, three hidden layers, and an output layer. The sizes of input and output layer are 1936 and 4, representing the 1936 bands in the input spectrum and 4 types of oil, respectively. Each of the hidden layers includes 512 neurons. The activation function between hidden layers is Rectified linear unit [37], and that of output layer is a sigmoid function. The initial learning rate is set at 0.001, and reduces at a factor of 10 after 200 iterations. The maximum number of iterations is set at 1000.

4) DNN With Differential Pooling: The hyperspectral sensor applied in the experiment obtains reflectance spectra with high spectral resolution. Like other hyperspectral remote sensing approach, the collected data include redundant bands, which increase computational complexity of the DNN model, and potentially cause the problem of collinearity during regression analysis. In order to reduce dimensionality of the hyperspectral data without losing necessary information, an additional differential pooling layer is applied to input spectra before DNN. This differential pooling layer integrates data pooling method with feature selection, and applies different pooling size based on the distribution of characteristic bands.

According to the report by Yang et al. [1] and the observations in the experiments of this article, blue-light bands from about 435 nm to about 580 nm have two strong reflection peaks and an absorption peak in between, which makes it a characteristic range for distinguishing oil types. Therefore, the size of pooling layer is relatively small in this range at 2 pixels, while that in the rest part of the spectra is relatively large at 10 pixels. The size of input spectrum is reduced to 262 bands after the differential pooling. The optimized input spectra are then fed to a DNN with same number of hidden layers and neurons, but reduced number of input size. The working flow of RF applied in this article is shown as Fig. 3(d).

III. Results and Discussion

A. Interpreting Reflectance Spectra of Oil Slick

The reflectance spectra collected for different types of oil under different thicknesses and wind conditions are shown in Fig. 4, and the reflectance spectra under different sunlight elevation angle (using 10.23 μm crude oil under no wind condition) is shown in Fig. 5. An absorption peak at around 745 nm and a reflection peak at 830 nm are observed in all the results, which generally conforms with the measurements by Lu et al. [14]. The results also show that the measured reflectance spectra are affected by slick thickness, wind condition, and incident angle. Generally speaking, the reflectances decrease with the increase of slick thickness, incident light angle, and additional wind

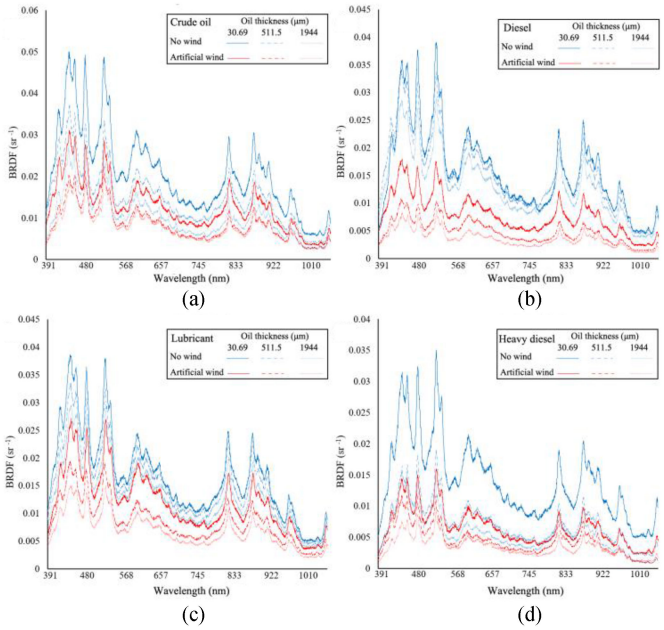

Fig. 4. Reflectance spectra collected under different slick thickness and wind conditions for four types of oil. (a) Crude oil. (b) Diesel. (c) Lubricant. (d) Heavy diesel.

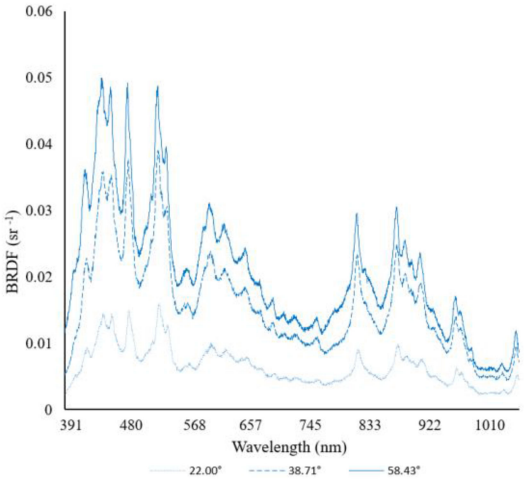

Fig. 5. Reflectance spectra collected for 1.944 mm crude oil under different sunlight elevation angle.

condition. It is difficult to detect the patterns in the reflectance spectra directly through human eyes.

As shown in Fig. 4, wind condition has significant influence on the reflectance spectra. Compared with calm condition, wind increases the roughness of oil slick surface. According to the microplane theory of BRDF, the incident photons are reflected more evenly to other directions with the increase of surface roughness [38]. As a result, the reflectances decrease with the increase of wind condition. This result generally confirms with the simulations and experiments by Otremba and Piskozub [27].

Oil thickness also has a negative correlation with the reflectance. Considering the movement of photons in the air-oil-water three-layer model, the thinner the oil slick is, the easier it

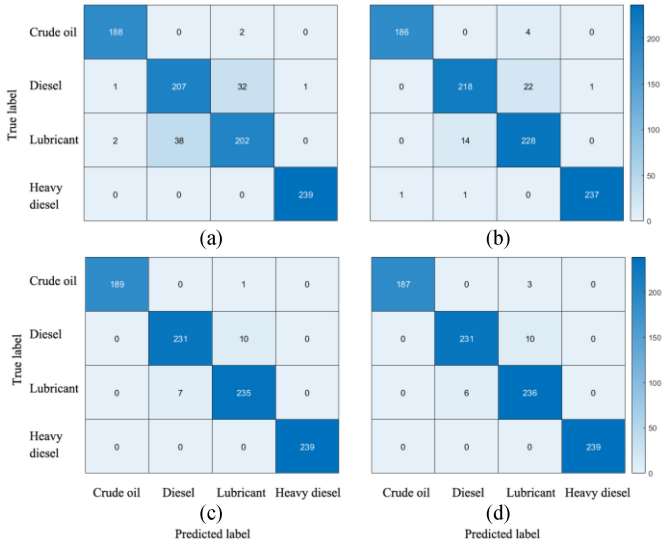

Fig. 6. Confusion matrix of test results for the four machine learning models. (a) Random forest. (b) Support vector machine. (c) Deep neural network. (4) DNN with differential pooling.

TABLE II
USERS', PRODUCERS', AND OVERALL ACCURACIES OF IDENTIFICATION RESULTS FOR FOUR MACHINE LEARNING MODELS

		RF	SVM	DNN	DP-DNN
Crude oil	PA	0.9895	0.9789	0.9947	0.9842
	UA	0.9843	0.9947	1.0000	1.0000
	OA	0.9945	0.9945	0.9989	0.9967
Diesel	PA	0.8589	0.9046	0.9585	0.9585
	UA	0.8449	0.9356	0.9706	0.9747
	OA	0.9211	0.9583	0.9814	0.9825
Lubricant	PA	0.8347	0.9421	0.9711	0.9752
	UA	0.8559	0.8976	0.9553	0.9478
	OA	0.9189	0.9561	0.9803	0.9792
Heavy diesel	PA	1.0000	0.9916	1.0000	1.0000
	UA	0.9958	0.9958	1.0000	1.0000
	OA	0.9989	0.9967	1.0000	1.0000

is for the photons to be reflected from the oil-water boundary, transmit through oil-air boundary, and finally reach the sensor. As a result, the reflectances decrease with the increase of oil thickness. This result generally confirms with the simulations and experiments by Ren et al. [30]. These results follow the theoretical basis of optical reflectance and conform with the measurements in previous study. Thus, they indicate the reliability of the collected data.

B. Comparisons Between Machine Learning Models

The accuracy of machine learning models is evaluated through producers' accuracies (PA), users' accuracies (UA), and overall accuracies (OAs), as well as the standard performance measurements: true positive rate (TPR); true negative rate (TNR); false positive rate (FPR); and false negative rate (FNR). The confusion matrixes of the classification results using different machine learning models are shown in Fig. 6. Based on the confusion matrix, PA, UA, and OA for each type of oil are given in Table II, and the corresponding performance measurements are given in

TABLE III
PERFORMANCE MEASUREMENT OF IDENTIFICATION RESULTS FOR FOUR MACHINE LEARNING MODELS

		RF	SVM	DNN	DP-DNN
Crude oil	TPR	0.9895	0.9789	0.9947	0.9842
	TNR	0.9958	0.9986	1.0000	1.0000
Diesel	TPR	0.8589	0.9046	0.9585	0.9585
	TNR	0.9434	0.9776	0.9896	0.9911
Lubricant	TPR	0.8347	0.9421	0.9711	0.9752
	TNR	0.9493	0.9612	0.9836	0.9806
Heavy diesel	TPR	1.0000	0.9916	1.0000	1.0000
	TNR	0.9985	0.9985	1.0000	1.0000

TABLE IV
NUMBER OF CALCULATIONS AND RUNNING TIME DURING THE TRAINING PROCESSES OF THE FOUR MACHINE LEARNING MODELS

	RF	SVM	DNN	DP-DNN
Number of calculations	5.21×10^4	9.37×10^4	5.52×10^7	3.04×10^6
Running time (s)	6.2	8.3	95	39

Table III. It should be noted that only TPR and TNR are shown in the table, since TPR+FPR = 1 and TNR+FNR = 1.

The performances of the four machine learning models are compared in terms of both accuracy and computational complexity. In term of the accuracy, all the four models are able to identify the two types of heavy oil. According to Fig. 6(a), however, RF model is not able to distinguish between the two types of light oil very well. The SVM model is able to achieve more accurate classification for the two types of light oil than the RF model. The DNN model and that with differential pooling provide classification results with similar accuracies, which are also more accurate than those of RF and SVM models. They are able to distinguish the two types of light oil more accurately than the other two machine learning models.

The number of the calculations and running time for the model training process is given in Table IV. The difference in the computational complexity between RF and SVM is not significant. The two DNN models, however, is much more complicated than RF and SVM. The number of calculations and training time for the DNN model and the other two models are at different orders of magnitude. In other words, the DNN models achieve more accurate identification results at the cost of higher computational complexity. Compared between the two DNN models, the one designed in this article with differential pooling involved smaller numbers of calculation because it reduces the number of parameters in input layer through dimensionality reduction. In other words, DP-DNN is able to achieve highly accurate prediction with less running time.

IV. CONCLUSION AND FUTURE STUDY

This article verifies and compares the ability of oil-type recognition using different machine learning models. The results show that all the four machine learning models are able to identify oil types based on high-resolution reflectance spectra under sunny weather and appropriate range of sunlight elevation angle. The regular DNN model is able to achieve accurate classification at the cost of more calculations and longer training time. Additionally, a DP-DNN, which includes a biased dimensionality reduction based on the characteristics of oil surface reflectance, is designed and implemented in this article. The results shown that the proposed model is able to classify oil types as accurately as the regular DNN model, but with smaller number of calculations. Therefore, the two DNN models would be the ideal choice for oil-types identification when the training time is sufficient. The SVM model, or the DNN model with differential pooling, which are able to achieve reasonable identification result with smaller number of calculations, may be a favorable choice to classify oil spill types using spectral data when training time is limited.

Since the different types of oil samples are put separately in beakers, the studies on the spectral response of mixed oil samples would be an interesting topic in our future study. Spectral unmixing method [40] may be adopted to solve this problem. For example, an unmixing model may be developed to simulate relation between the reflectance spectra of different types of oil and those of the mixture.

It should also be noted that the hyperspectral sensor used in this article has a much higher spectral resolution than any existing satellite-based (usually less than 20 bands) or airborne (usually less than 300 bands) hyperspectral sensor, and obtains accurate spectral radiance in relatively small vision field with minor distortion caused by center wavelength shift or band-to-band misregistration ("smile" and "keystone" properties), which are commonly witnessed in unprocessed satellite-based HSI [39]. Examining the models' performances using the data with coarser spectral resolution, and further verifying their prediction with existing satellite-based or airborne hyperspectral data would also be a topic of our near future study.

A potential method of improving the classification model and applying it with coarser hyperspectral data would be a remote sensing data fusion approach that combines reflectance spectra with polarization imaging. Since the polarization characteristics of oil surface are able to reveal more information about the roughness and texture than using reflectance spectra along [41], they have been applied to the field of oil spill detection [42]–[44]. Therefore, we envision a fusion approach which may be able to distinguish between different types of oil that have similar reflectance spectra, and achieve accurate classification using hyperspectral data with coarser bands.

ACKNOWLEDGMENT

The authors would like to thank W. Zheng from Dalian Maritime University for the help in preparing the training dataset. The author would also like to thank G. Wang from Dalian Maritime University for providing oil samples. The authors are grateful to the anonymous reviewers for their constructive comments on this article.

REFERENCES

[1] J. Yang, J. Wan, Y. Ma, J. Zhang, and Y. Hu, "Characterization analysis and identification of common marine oil spill types using hyperspectral remote sensing," *Int. J. Remote Sens.*, vol. 41, no. 18, pp. 7163–7185, Jun. 2020.

[2] S. Qayum and W. Zhu, "An overview of international and regional laws for the prevention of marine oil pollution and 'international obligation of Pakistan," *Indian J. Geo-Marine Sci.*, vol. 47, no. 3, pp. 529–539, Mar. 2018.
[3] M. Fingas and C. E. Brown, "A review of oil spill remote sensing," *Sensors*, vol. 18, no. 1, Jan. 2018, Art. no. 91.
[4] C. C. Texeira *et al.*, "Source identification of sea surface oil with geochemical data in Cantarell, Mexico," *Microchem. J.*, vol. 117, pp. 202–213, Nov. 2014.
[5] J. M. Bayona, C. Domínguez, and J. Albaigés, "Analytical developments for oil spill fingerprinting," *Trends Environ. Anal. Chem.*, vol. 5, pp. 26–34, Feb. 2015.
[6] Z. Cheng, Y. Wang, F. Wang, Y. Wang, and Y. Zhou, "Excitation-emission matrix spectroscopy and parallel factor analysis for micro-content petroleum pollutant," *Spectroscopy Spectral Anal.*, vol. 34, no. 9, pp. 2561–2567, Sep. 2014.
[7] Y. Hou, Y. Li, B. Liu, and T. Wang, "Design and implementation of a coastal-mounted sensor for oil film detection on seawater," *Sensors*, vol. 18, no. 1, Jan. 2018, Art. no. 70.
[8] S. Sun *et al.*, "Oil slick morphology derived from AVIRIS measurements of the deepwater horizon oil spill: Implications for spatial resolution requirements of remote sensors," *Marine Pollut. Bull.*, vol. 103, pp. 276–285, Feb. 2016.
[9] Y. Lu *et al.*, "Optical interpretation of oil emulsions in the ocean – part I: Laboratory measurements and proof-of-concept with AVIRIS observations," *Remote Sens. Environ.*, vol. 230, Sep. 2019, Art. no. 111183.
[10] Y. Lu, J. Shi, C. Hu, M. Zhang, S. Sun, and Y. Liu, "Optical interpretation of oil emulsions in the ocean – Part II: Applications to multi-band coarse-resolution imagery," *Remote Sens. Environ.*, vol. 242, Jun. 2020, Art. no. 111778.
[11] R. N. Clark *et al.*, "Imaging spectroscopy: Earth and planetary remote sensing with the USGS tetracorder and expert systems," *J. Geophys. Res.*, vol. 108, no. E12, Dec. 2003, Art. no. 5131.
[12] R. N. Clark, J. M.Curchin, T. M. Hoeffen, and G. A. Swayze, "Reflectance spectroscopy of organic compounds: 1 Alkanes," *J. Geophys. Res.*, vol. 114, Mar. 2009, Art. no. E03001.
[13] R. N. Clark *et al.*, "A method for quantitative mapping of thick oil spills using imaging spectroscopy," 2010.
[14] Y. Lu, Q. Tian, J. Wang, X. Wang, and Qi X, "Experimental study on spectral responses of offshore oil slick," *Chin. Sci. Bull.*, vol. 53, no. 24, pp. 3937–3941, Dec. 2008.
[15] T. Lammoglia and C. R. S. Filho, "Spectroscopic characterization of oils yielded from Brazilian offshore basins: Potential applications of remote sensing," *Remote Sens. Environ.*, vol. 115, pp. 2525–2535, Oct. 2011.
[16] B. Liu, Y. Li, and X. Zhu, "Assessing the capabilities of hyperspectral remote sensing to map oil films on waters," *Proc. SPIE,* vol. 9299, 2014, Art. no. 929902.
[17] L. Zhang, L. Zhang, and B. Du, "Deep learning for remote sensing data: A technical tutorial on the state of the art," *IEEE Geosci. Remote Sens. Mag.*, vol. 4, no. 2, pp. 22–40, Jun. 2016.
[18] X. X. Zhu, D. Tuia, L. Mou, G. S. Xia, F. Xu Zhang, and F. Fraundorfer, "Deep learning in remote sensing: A comprehensive review and list of resources," *IEEE Geosci. Remote Sens. Mag.*, vol. 5, no. 4, pp. 8–36, Dec. 2017.
[19] W. Chang, B. Liu, and Q. Zhang, "Oil slick extraction from hyperspectral images using a modified stacked auto-encoder network," *Proc. SPIE,* vol. 11179, 2019, Art. no. 1117931.
[20] B. Liu, Q. Zhang, Y. Li, W. Chang, and M. Zhou, "Spatial–spectral jointed stacked auto-encoder-based deep learning for oil slick extraction from hyperspectral images," *J. Indian Soc. Remote Sens.*, vol. 47, no. 12, pp. 1989–1997, Dec. 2019.
[21] B. Liu, Y. Li, G. Li, and A. Liu, "A spectral feature based convolutional neural network for classification of sea surface oil spill," *ISPRS Int. J. Geo-Inf.*, vol. 8, no. 4, Mar. 2019, Art. no. 160.
[22] X. Zhu, Y. Li, Q. Zhang, and B. Liu, "Oil film classification using deep learning-based hyperspectral remote sensing technology," *ISPRS Int. J. Geo-Inf.*, vol. 8, no. 4, Apr. 2019, Art. no. 181.
[23] J. Menezes and N. Poojary, "A fusion approach to classify hyperspectral oil spill data," *Multimed. Tools Appl.*, vol. 79, pp. 5399–5418, Oct. 2018.
[24] Y. Chen, L. Huang, L. Zhu, N. Yokoya, and X. Jia, "Fine-grained classification of hyperspectral imagery based on deep learning," *Remote Sens.,* vol. 11, no. 22, Nov. 2019, Art. no. 2690.
[25] F. E. Nicodemus, "Reflectance nomenclature and directional reflectance and emissivity," *Appl. Opt.*, vol. 9, no. 6, pp. 1474–1475, 1970.
[26] Z. Otremba and J. Piskozub, "Modelling of the optical contrast of an oil film on a sea surface," *Opt. Express*, vol. 9, no. 8, pp. 411–416, Oct. 2001.
[27] Z. Otremba and J. Piskozub, "Modelling the bidirectional reflectance distribution functions (BRDF) of seawater polluted by an oil film," *Opt. Express*, vol. 12, no. 8, pp. 1671–1676, Apr. 2004.
[28] Z. Otremba, "Modelling the bidirectional reflectance distribution functions (BRDF) of sea areas polluted by oil," *Oceanologia*, vol. 46, no. 4, pp. 505–518, Sep. 2004.
[29] Z. Otremba, "Influence of oil dispersed in seawater on the bi-directional reflectance distribution function (BRDF)," *Optica Applicata*, vol. 35, no. 1, pp. 99–109, 2005.
[30] Z. Ren, C. Ma, L. Chen, and G. Chen, "Modeling and simulating the bidirectional reflectance distribution function (BRDF) of seawater covered by oil slicks," *J. Modern Opt.*, vol. 63, no. 9, pp. 913–920, Oct. 2015.
[31] L. Breiman, "Random forests," *Mach. Learn.*, vol. 45, no. 1, pp. 5–31, 2001.
[32] A. Liaw and M. Wiener, "Classification and regression by randomforest," *R News*, vol. 2/3, pp. 18–22, Dec. 2002.
[33] M. Belgiu and L. Dragut, "Random forest in remote sensing: A review of applications and future direction," *ISPRS Int. J. Photogramm. Remote Sens.*, vol. 114, no. 3, pp. 24–31, Apr. 2016.
[34] C. Cortes and V. Vapnik, "Support-vector networks," *Mach. Learn.*, vol. 20, no. 3, pp. 273–297, 1995.
[35] H. Yu, "Support vector machine," in *Encyclopedia of Database Systems*, L. Liu and M. Tamer ÖZSU, Eds. Boston, MA, USA: Springer, 2009.
[36] R. M. Rifkin and A. Klautau, "In defense of one-vs-all classification," *J. Mach. Learn. Res.*, vol. 5, pp. 101–141, Jan. 2004.
[37] V. Nair and G. E. Hinton, "Rectified linear units improve restricted Boltzmann machines," in *Proc. 27th Int. Conf. Mach. Learn.*, Jun. 2010, pp. 807–814.
[38] V. Ross, D. Dion, and G. Potvin, "Detailed analytical approach to the Gaussian surface bidirectional reflectance distribution function specular component applied to the sea surface," *J. Opt. Soc. Amer. A*, vol. 22, no. 11, pp. 2442–2453, Nov. 2005.
[39] N. Yokoya, N. Miyamura, and A. Iwasaki, "Preprocessing of hyperspectral imagery with consideration of smile and keystone properties," *Proc. SPIE,* vol. 7857, Oct. 2010, Art. no. 78570B.
[40] P. Sidike, J. Khan, M. Alam, and S. Bhuiyan, "Spectral unmixing of hyperspectral data for oil spill detection," *Proc. SPIE,* vol. 8498, Oct. 2012, Art. no. 84981B.
[41] D. A. Talmage and P. J. Curran, "Remote sensing using partially polarized light," *Int. J. Remote Sens.*, vol. 7, no. 1, pp. 47–64, 1986.
[42] Z. Sun, Y. Zhao, G. Yan, and Li S, "Study on the hyperspectral polarized reflection characteristics of oil slicks on sea surfaces," *Chin. Sci. Bull.*, vol. 55, pp. 2771–2776, 2010.
[43] H.-Y. Shen, P.-C. Zhou, and S.-R Feng, "Research on multi-angle near infrared spectral-polarimetric characteristic for polluted water by spilled oil," *Proc. SPIE,* vol. 8193, Sep. 2011, Art. no. 81930M.
[44] A. L. Iler and P. D. Hamilton, "Detecting oil on water using polarimetric imaging," *Proc. SPIE,* vol. 9459, May 2015, Art. no. 94590P.

Ying Li received the Ph.D. degree in geographic information science from Tohoku University, Miyagi, Japan, in 1996.

She is currently a professor with Navigation College, Dalian Maritime University, China, and the Dean of Environmental Information Institute, Dalian Maritime University. Under the authorization of ESRI, she set up teaching and research center of ArcGIS in Dalian Maritime University. She has been committed to the research and application of GIS and remote sensing technology in oceanic environment and maritime transportation, as well as the detection technology of oil pollution.

Dr. Li invention of oil spill detection instrument based on remote sensor is the recipient of the second prize of National Technological Invention Award of China.

Qinglai Yu received the B.Sc degree in computer science from Harbin Engineering University, Harbin, China, in 2016. He is currently working toward the Master's degree with the Navigation College, Dalian Maritime University, Dalian, China.

His current research interests include the interpretation of hyperspectral remote sensing data, and the applications of remote sensing technology in marine transportation.

Ming Xie received the B.Sc. degree in physical geography from Nanjing University, Nanjing, China, in 2008, and the M.S. and the Ph.D. degrees in geographic information science from the University of South Florida, Tampa, FL, USA, in 2019.

He is currently an Instructor with Navigation College, Dalian Maritime University, Dalian, China. He is aiming at the cross-boundary researches between advanced machine learning method and modern remote sensing technology. His current research interests include the applications of advanced machine learning method in hyperspectral remote sensing image processing and object detection, as well as the application of GIS and RS technology in coastal environment and transportation.

Zhenduo Zhang received the Ph.D. degree in optical engineering from Chinese Academy of Sciences, Changchun, China, in 2010. From 2010 to 2019, he was a Research Assistant with Chengchun Institution of Optics, Fine Mechanics and Physics, Chinese Academy of Sciences, Chuangchun, China. He is currently a Professor with Navigation College, Dalian Maritime University, Dalian, China. His current research interests include physical model of reflectance spectrum, the interpretation of hyperspectral remote sensing data, and optical design for optical remote sensor.

Zhanjun Ma received the B.Sc degree in electronic engineering from Tianjin University of Technology,Tianjin, China, in 2018. He is currently working toward the Master's degree with the Navigation College, Dalian Maritime University, Dalian, China.

His current research interests include numerical modeling of surface reflectance, and the spectral analysis of oil surface.

Kai Cao received the Master and Ph.D degrees in geology from Peking University, Beijing, China, in 2017.

He is currently a Postdoc Researcher with Navigation College, Dalian Maritime University, Dalian, China. His current research interests include advanced machine learning technology, and navigation visualization technology.